On the binary nature of the γ-ray sources AGL J2241+4454 (= MWC 656) and HESS J0632+057 (= MWC 148)

J. Casares,[1,2]★ M. Ribó,[3]★ I. Ribas,[4]★ J. M. Paredes,[3]★ F. Vilardell[5]★
and I. Negueruela[5]★

[1]*Instituto de Astrofísica de Canarias, E-38200 La Laguna, Tenerife, Spain*
[2]*Departamento de Astrofísica, Universidad de La Laguna, Avda. Astrofísico Francisco Sánchez s/n, E-38271 La Laguna, Tenerife, Spain*
[3]*Departament d'Astronomia i Meteorologia, Institut de Ciències del Cosmos (ICC), Universitat de Barcelona (IEEC-UB), Martí i Franquès 1, E-08028 Barcelona, Spain*
[4]*Institut de Ciències de l'Espai – (IEEC-CSIC), Campus UAB, Facultat de Ciències, Torre C5 - parell - 2a planta, E-08193 Bellaterra, Spain*
[5]*Departamento de Física, Ingeniería de Sistemas y Teoría de la Señal, Universidad de Alicante, Apdo. 99, E-03080 Alicante, Spain*

ABSTRACT

We present optical spectroscopy of MWC 656 and MWC 148, the proposed optical counterparts of the γ-ray sources AGL J2241+4454 and HESS J0632+057, respectively. The main parameters of the Hα emission line [equivalent width (EW), full width at half-maximum and centroid velocity] in these stars are modulated on the proposed orbital periods of 60.37 and 321 d, respectively. These modulations are likely produced by the resonant interaction of the Be discs with compact stars in eccentric orbits. We also present radial velocity curves of the optical stars folded on the above periods and obtain the first orbital elements of the two γ-ray sources, thus confirming their binary nature. Our orbital solution supports eccentricities $e \sim$ 0.4 and 0.83 ± 0.08 for MWC 656 and MWC 148, respectively. Furthermore, our orbital elements imply that the X-ray outbursts in HESS J0632+057/MWC 148 are delayed $\sim$0.3 orbital phases after periastron passage, similar to the case of LS I +61 303. In addition, the optical photometric light-curve maxima in AGL J2241+4454/MWC 656 occur $\sim$0.25 phases passed periastron, similar to what is seen in LS I +61 303. We also find that the orbital eccentricity is correlated with the orbital period for the known γ-ray binaries. This is explained by the fact that small stellar separations are required for the efficient triggering of very high energy radiation. Another correlation between the EW of Hα and orbital period is also observed, similar to the case of Be/X-ray binaries. These correlations are useful to provide estimates of the key orbital parameters $P_{\rm orb}$ and e from the Hα line in future Be γ-ray binary candidates.

Key words: stars: emission-line, Be – stars: individual: MWC 656 – stars: individual: MWC 148 – gamma rays: stars – X-rays: stars.

1 INTRODUCTION

Cherenkov telescopes are opening a new era of discoveries with the detection of large populations of γ-ray sources ranging from Galactic objects (supernova remnants, pulsar-wind nebulae and compact binaries) to distant blazars and starburst galaxies (Hinton & Hofmann 2009). In particular, the class of γ-ray binaries has attracted great attention in the last few years. They are characterized by the presence of a compact star orbiting a late-O/early-B companion. Either if particles are accelerated in a microquasar jet or in the collision of two winds, the high density of ultraviolet (UV) photons from the massive star provides the necessary environment for the production of GeV–TeV emission through inverse Compton scattering. There are currently three confirmed γ-ray binaries with high energy (HE; $E > 100$ MeV) and/or very high energy (VHE; $E > 100$ GeV) emission modulated on the orbital period: PSR B1259−63, LS 5039 and LS I +61 303 (Paredes 2011). Three more candidates have been recently proposed but their binary nature awaits confirmation. These are 1FGL J1018.6−5856 (Corbet et al. 2011), AGL J2241+4454 and HESS J0632+057. The latter two sources are the subject of this paper.

AGL J2241+4454 is a point-like γ-ray source detected by the *AGILE* satellite above 100 MeV (Lucarelli et al. 2010). The error circle of the satellite contains the Be star MWC 656 (=HD 215227)

★E-mail: jorge.casares@iac.es (JC); mribo@am.ub.es (MR); iribas@ieec.uab.es (IR); jmparedes@ub.edu (JMP); vilardell@ice.cat (FV); ignacio@dfists.ua.es (IN)

which was proposed by Williams et al. (2010) as the likely optical counterpart. The same authors suggest a spectral classification B3 IVne+sh and an orbital period of 60.37±0.04 d based on *Hipparcos* light-curve data. By fitting the spectral energy distribution in the UV and *B* band a distance of 2.6 ± 1.0 kpc is derived. This, combined with its high Galactic latitude $b = -12°$, implies a runaway star, another evidence supporting its binary nature.

On the other hand, MWC 148 (=HD 259440) is a B0 Vpe star which has been proposed as the optical counterpart of the TeV source HESS J0632+057 (Aharonian et al. 2007). The claim is based on the detection of radio (Skilton et al. 2009) and X-ray emission associated with MWC 148 (Hinton et al. 2009; Falcone et al. 2010) with similar spectral indices and variability as observed in PSR B1259−63, LS 5039 and LS I +61 303. Recently, extended and variable radio emission at au scales, showing similar morphology to these three γ-ray binaries, has been reported (Moldón, Ribó & Paredes 2011a; see also Dhawan et al. 2006; Ribó et al. 2008 and Moldón et al. 2011b). Lower limits to the orbital period of >54 d (Falcone et al. 2010) and >200 d (Casares et al. 2011) were proposed based on X-ray and optical emission-line variability. Furthermore, the absence of significant radial velocity shifts in the B0 star supports a long period >100 d (Aragona, McSwain & De Becker 2010). Finally, Bongiorno et al. (2011) report the presence of strong X-ray flares in *Swift* X-Ray Telescope (*Swift*/XRT) data, modulated with a period of 321 ± 5 d which strongly advocates for its binary nature.

Alternative scenarios to the binary hypothesis invoke an isolated star where HE emission is produced in a wind-driven shock. In particular, Bp stars are known to possess strong surface magnetic fields which efficiently confine the stellar wind and may accelerate particles up to TeV energies (Townsend, Owocki & Ud-Doula 2007). The best way to test the binary model and solve the system geometry is through a radial velocity study and hence we have embarked in an optical spectroscopic campaign of MWC 656 and MWC 148 using several telescopes. Our analysis demonstrates that these stars are indeed the optical companions of high-mass X-ray binaries (HMXBs)/γ-ray binaries responsible for the HE/VHE emission of AGL J2241+4454 and HESS J0632+057. In the following sections we present the observations, our best constraints to the orbital parameters and discussion of results.

2 OBSERVATIONS

2.1 MWC 656

We observed MWC 656 using the Fibre-fed RObotic Dual-beam Optical Spectrograph (FRODOspec) on the robotic 2.0-m Liverpool Telescope (LT) at the Observatorio del Roque de Los Muchachos between 2011 April 23 and July 28. The spectrograph is fed by a fibre bundle array consisting of 12 × 12 lenslets of 0.82 arcsec each, which is reformatted as a slit. The spectrograph was operated in a high-resolution mode, providing a dispersion of 0.35 Å pixel^{-1} and spectral resolving power $R \sim 5500$ in the blue arm, while 0.80

Å pixel^{-1} and $R \sim 5300$ in the red arm. The spectral coverage was 3900–5215 and 5900–8000 Å, respectively. A total of 32 600 s spectra were obtained with the blue arm and 64 290 s spectra with the red arm. One blue and two red spectra were obtained on each observing night. A log of the observations is presented in Table 1. The FRODOspec pipeline produces fully extracted and wavelength-calibrated spectra with rms ≤ 0.1 Å above 4400 Å. The analysis presented in this paper has been performed with the FRODOspec pipeline products.

2.2 MWC 148

MWC 148 was observed with the Intermediate dispersion Spectrograph (IDS) attached to the 2.5-m Isaac Newton Telescope (INT) at the Observatorio del Roque de Los Muchachos on the nights of 2008 October 20–23. A total of 35 spectra were obtained in the blue spectral range (3900–5500 Å, unvignetted) using the R900V grating in combination with the 235-mm camera and a 1.2 arcsec slit to provide a spectral resolution of 80 km s^{-1} [full width at half-maximum (FWHM)]. Nightly averages were produced from the individual spectra resulting in a total of three INT spectra.

12 additional blue spectra were obtained on the nights of 2008 December 7–8 and 10–11 with the Intermediate dispersion Spectrograph and Imaging System (ISIS) double-arm spectrograph on the William Herschel Telescope (WHT). Here we employed the 600B and 1200B gratings on the blue arm resulting in the wavelength coverages of 3800–5400 and 3700–4500 Å, respectively. A 1 arcsec slit was selected yielding spectral resolutions in the range of 65–115 km s^{-1}. Meanwhile, the 600R and 1200R gratings were mounted on the ISIS red arm, centred at different wavelengths, to yield simultaneous spectra in the Hα and Ca II NIR triplet. Nightly averages were produced for the different spectral configurations.

The High Efficiency and Resolution Mercator Echelle Spectrograph (HERMES) on the 1.2-m Mercator (MT) telescope was also used to obtain three nightly 1800 s spectra on the nights of 2009 October 30–31, November 1–4 and 6–8. HERMES is a fibre-fed spectrograph and we employed the high-resolution mode which yield a resolving power $R = 85\,000$ across the entire optical range between 3770 and 9000 Å. The signal-to-noise ratio in the HERMES spectra is significantly lower than in the INT and WHT data, so we decided to co-add the three individual spectra obtained every night resulting in a total of nine Mercator spectra.

22 high-resolution *Echelle* spectra were also obtained during the period 2010 January 20–April 8 using the fibre-fed STELLA Echelle Spectrograph (SES) of the 1.2-m robotic STELLA-I (ST) telescope at the Observatorio del Teide in Tenerife. The spectra cover the wavelength range of 3870–8800 Å with increasing inter-order gaps starting at 7200 Å. The spectrograph provides an effective resolving power $R = 55\,000$. One spectrum was obtained per night and the exposure time was set to 1800 s.

Finally, MWC 148 was also observed with FRODOspec at the LT between 2010 September 4 and 2011 May 3 using the same configuration as for MWC 656 (see above). One 600 s spectrum

Table 1. Log of the MWC 656 observations.

Date	Telescope	Spectral range (Å)	Number of spectra	Exposure time (s)	Dispersion (Å pixel^{-1})
2011 April 23–July 28	LT	3900–5215	32	600	0.35
2011 April 23–July 28	LT	5900–8000	64	290	0.80

Table 2. Log of the MWC 148 observations.

Date	Telescope	Spectral range (Å)	Number of spectra	Exposure time (s)	Dispersion (Å pixel^{-1})
2008 October 20	INT	3900–5500	10	90	0.63
2008 October 21	INT	3900–5500	5	90	0.63
2008 October 22	INT	3900–5500	10, 10	120, 90	0.63
2008 December 7	WHT	3800–5400	3	20	0.88
2008 December 7	WHT	8300–8960	3	20	0.99
2008 December 8	WHT	3800–5400	3	20	0.88
2008 December 8	WHT	5555–7070	3	20	0.99
2008 December 10	WHT	3700–4500	3	25	0.45
2008 December 10	WHT	8335–9075	3	15	0.48
2008 December 11	WHT	3700–4500	3	25	0.45
2008 December 11	WHT	8335–9075	3	15	0.48
2009 October 30–November 8	MT	3770–9000	27	1800	0.02
2010 January 20–April 8	ST	3870–8800	22	1800	0.10
2010 September 4–2011 May 3	LT	3900–5215	40	600	0.35
2010 September 4–2010 October 20	LT	5900–8000	48	193	0.80
2010 October 24–2011 May 3	LT	5900–8000	47	290	0.80

and two 290 s or three 193 s red spectra were obtained per night. A full log of the observations is presented in Table 2.

The INT, WHT and MT spectra were reduced using standard techniques including debiasing and flat-fielding. The spectra were subsequently extracted using optimal extraction techniques in order to optimize the signal-to-noise ratio of the output (Horne 1986). Frequent observations of comparison arc lamp or hollow cathode lamp images were performed in the course of each run and the pixel-to-wavelength scale was derived through polynomial fits to a large number of identified reference lines. The final rms scatter of the fit was always <1/30 of the spectral dispersion. The automatic pipeline products were used for the ST and the LT data.

The spectral-type standard HR 2479 (B0 III) was also observed with all different telescopes and instrument configurations for the purpose of computing the rotational broadening of the companion star. It was selected because of its low projected rotational velocity of 50 km s^{-1} (Abt, Levato & Grosso 2002).

3 DESCRIPTION OF THE SPECTRA AND ROTATIONAL BROADENING

All the spectra were rectified by dividing a low-order spline fit to the continuum. For comparison, Fig. 1 displays the averaged normalized LT spectra of MWC 148 and MWC 656. Both targets show similar spectra, with very broad and shallow photospheric absorption lines. Strong Balmer emission is seen out to Hβ in MWC 656 and to Hγ in MWC 148. The Hβ line shows a double-peaked profile characteristic of circumstellar discs. Several Fe II disc emission lines are also detected. In summary, both spectra are typical of early-type Be stars with well-developed discs fed by stable mass-loss (Porter & Rivinius 2003). Detailed spectral analyses performed by Williams et al. (2010) and Aragona et al. (2010) support a spectral classification B3 IVne+sh for MWC 656 and B0 Vpe for MWC 148. In the remaining of this paper we have adopted the spectral classification and stellar parameters derived in these works.

Projected rotational velocities of 430 km s^{-1} (Gutiérrez-Soto et al. 2007) and 500 km s^{-1} (Aragona et al. 2010) have been reported for MWC 148, whereas 262 ± 26 km s^{-1} (Yudin 2001) and 300 ± 50 km s^{-1} (Williams et al. 2010) for MWC 656. We decided
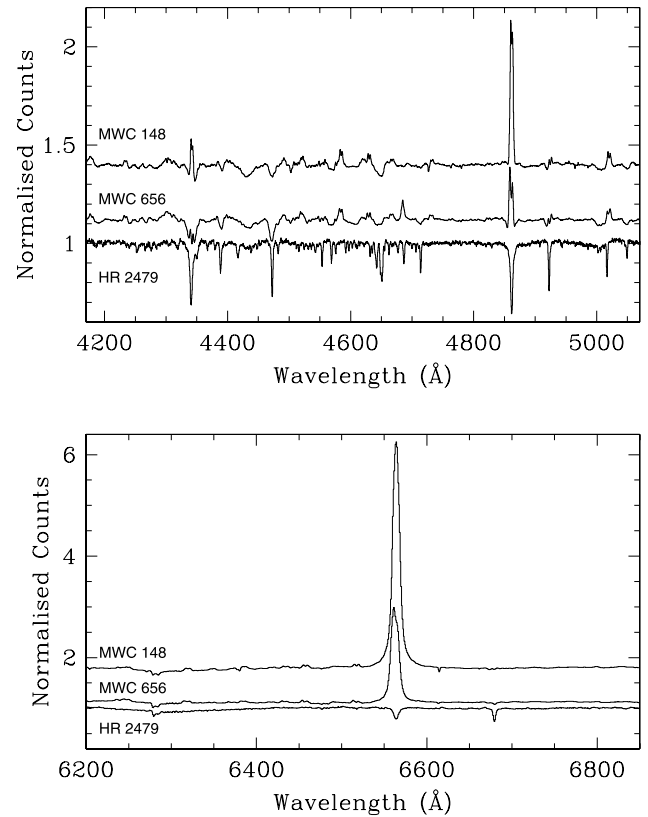

Figure 1. Average LT spectra of MWC 148 and MWC 656 in the blue (top panel) and red (bottom panel) spectral regions. The bottom spectra show the B0 III star HR 2479 for comparison, which has an intrinsic broadening of 50 km s^{-1}.

to estimate the rotational broadening $v \sin i$ from our own spectra following the technique outlined in Marsh, Robinson & Wood (1994), which basically subtracts broadened templates from the average spectrum of the target and searches for the lowest residual. Therefore, we first rebinned our LT spectra of the two stars and the template HR 2479 into a uniform velocity scale of 23 km s^{-1} pixel^{-1}. The template was subsequently broadened from 100 to
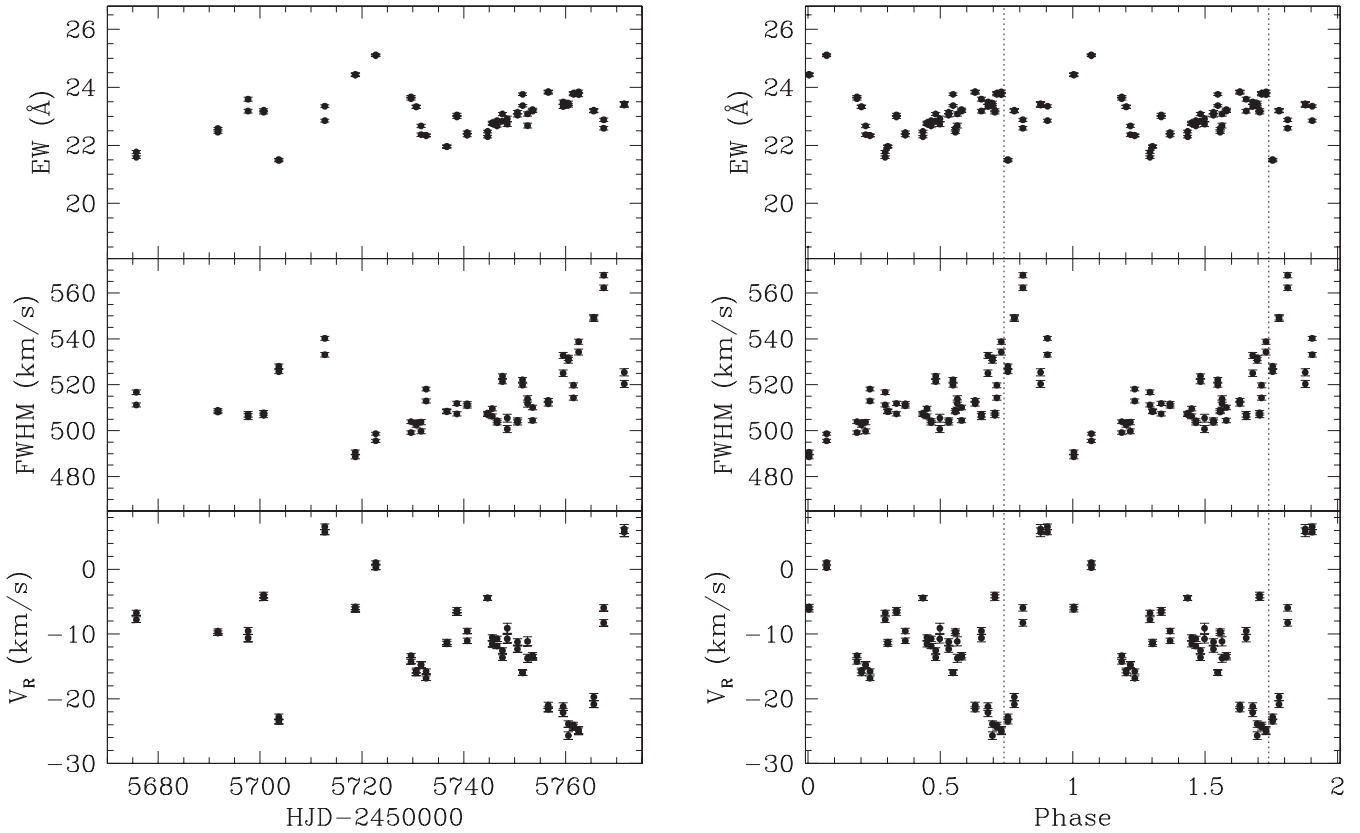
Figure 2. Left-hand panel: time evolution of the Hα-line parameters in MWC 656. Both the FWHM and centroid velocities show significant variability with maxima roughly separated by ∼60 d. Right-hand panel: same but folded on the 60.37 d period of Williams et al. (2010). Phase 0 has been set to the time of maximum optical brightness at HJD 2453243.3. The vertical dotted line denotes the phase of the periastron (see the text).

$500 \, \mathrm{km \, s^{-1}}$ in steps on $5 \, \mathrm{km \, s^{-1}}$ using a Gray rotational profile (Gray 1992) with a limb-darkening coefficient $\epsilon = 0.33$. The broadened versions of the template were multiplied by a scaling factor ≤ 1 to account for dilution due to extra sources of continuum light (such as the equatorial Be disc) and subtracted from the averaged spectra of the two targets. The subtraction was restricted to the blue spectral range of 4400–5200 Å, where the photospheric He I, He II and metallic lines are most prominent. The interstellar, Balmer and Fe II emission lines were all masked in the process. A χ^2 test on the residuals of the subtraction yields optimum rotational broadening of $370 \, \mathrm{km \, s^{-1}}$ for MWC 148 and $342 \, \mathrm{km \, s^{-1}}$ for MWC 656, with a formal uncertainty of $\pm 10 \, \mathrm{km \, s^{-1}}$. The rotational velocity of the template star needs to be added quadratically to these, resulting in $v \sin i = 373 \, \mathrm{km \, s^{-1}}$ for MWC 148 and $346 \, \mathrm{km \, s^{-1}}$ for MWC 656. The same analysis was repeated for MWC 148 using the other instrument configurations, and we always obtained values in the range of 355–$381 \, \mathrm{km \, s^{-1}}$.

4 ANALYSIS OF MWC 656

Be discs in X-ray binaries typically display not only the long-term superorbital variability associated with activity episodes, but also sometimes variability modulated with the binary orbital period (Zamanov et al. 1999). The strong Hα emission is the best tracer of disc variability and hence we decided to analyse several line parameters in MWC 656 and test whether they are modulated with the claimed 60.37 d orbital period (Williams et al. 2010). First, we measured the equivalent width (EW hereafter) by integrating

the Hα-emission profile in the 64 individual spectra. In addition, the FWHM and velocity shift of the line centroid were extracted through simple Gaussian fits. The left-hand panel of Fig. 2 presents the evolution of the Hα parameters with time. Because our base line extends over just 96 d, we cannot probe for the presence of a 60.37 d modulation through a period-search analysis.

The EW is fairly stable during our observations with a mean of $\sim$23 Å and a smooth increase towards the end of our observing window. A peak is detected at HJD 2455725 but, unfortunately, we lack the necessary time coverage to check for repeatability with a 60 d period. On the other hand, the FWHM and centroid velocity do display significant variability, with two maxima elapsed by $\sim$60 d, in good agreement with the photometric modulation of Williams et al. (2010). The behaviour of the Hα line parameters with the 60.37 d period is presented in the right-hand panel of Fig. 2.

Next, we attempted to measure radial velocities from the photospheric lines of the Be star. This is complicated by the fact that these lines are extremely broad and, in most cases, blended with disc emission lines e.g. the He I lines at 4922 and 5015 Å partly overlap with Fe II emissions at 4924 and 5018 Å (see Fig. 1). After careful comparison of the average spectrum of MWC 656 with the broadened template HR 2479, we decided to restrict the radial velocity analysis to three spectral windows covering the He I lines 4471, 4713 and 5048 Å. We measured radial velocities by cross-correlating each spectrum of MWC 656 with a template formed from the average of the entire data base. We find that this yields better results than using the broadened version of HR 2479 as template. The radial velocity of the template was determined by fitting
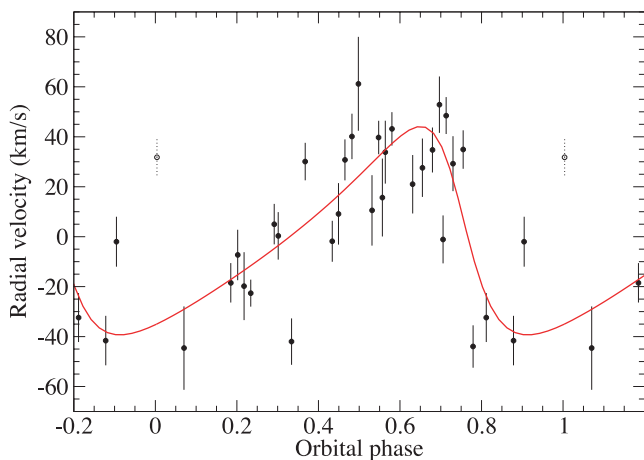
Figure 3. Radial velocity curve of MWC 656 folded on the 60.37 d period. The best-fitting solution, using an eccentric orbit with $e = 0.4$, is overplotted. The dotted point (at phase ∼0.0) has been masked from the fit. Phase 0 is set to HJD 2453243.3.

Table 3. Orbital solution for MWC 656 and MWC 148.

Parameter	MWC 656	MWC 148
P_{orb} (d)	60.37 (fixed)	321 (fixed)
T_0 (HJD $-2450\,000$)	3243.3 (fixed)	4857.5 (fixed)
e	0.4 (fixed)	0.83 ± 0.08
ω (°)	71 ± 23	129 ± 17
γ (km s^{-1})	-2.8 ± 9.4	48.3 ± 8.9
ϕ_{peri}	0.74 ± 0.05	0.967 ± 0.008
K_{opt} (km s^{-1})	41.7 ± 6.8	22.0 ± 5.7
$a_1 \sin i$ (R$_\odot$)	45.6 ± 7.3	77.6 ± 25.9
$f(M)$ (M$_\odot$)	$0.35^{+0.20}_{-0.15}$	$0.06^{+0.15}_{-0.05}$
σ (km s^{-1})	20.3	12.8

a Gaussian to the core of the He I 4471 Å line, and it was added to the velocities obtained from the cross-correlation. Fig. 3 presents the final radial velocities folded on the 60.37 d period of Williams et al. (2010). The plot reveals a sine-like modulation which hints for a moderate eccentricity.

The radial velocity curve was subsequently modelled with an eccentric orbital solution using the Spectroscopic Binary Orbit Program (SBOP; Etzel 2004). The orbital period was fixed to 60.37 d and phase 0 arbitrarily set to HJD 2453243.3 which corresponds to the epoch of maximum brightness in the photometric light curve (Williams et al. 2010). Individual points were weighted proportionally to $1/\sigma^2$, where σ is the radial velocity uncertainty. In the solutions, we adjusted the following orbital parameters: argument of the periastron (ω), systemic velocity (γ), phase of the periastron (ϕ_{peri}) and velocity semi-amplitude (K_{opt}). The solution does not converge if the orbit eccentricity (e) is left free. Therefore, we attempted several fits fixing the eccentricity by hand and found a minimum rms for $e = 0.4$. Fitting tests using several orbital configurations indicate that an uncertainty of ± 0.1 for $e = 0.4$ is appropriate. Note that we have masked the one discrepant point at phase 0 from the fit. A close look at this spectrum shows a flatter He I 4471 Å profile than the rest, possibly due to disc emission. In any case, this point has a marginal impact in the final solution since it slightly reduces the eccentricity to 0.35, while the remaining orbital parameters are virtually unaffected. Table 3 presents our final best-fitting parameters.

5 ANALYSIS OF MWC 148

In this section we repeat the previous analysis for the star MWC 148. The left-hand panel in Fig. 4 presents the behaviour of the main Hα parameters over our baseline of nearly three years. The LT data reveal a smooth sinusoidal modulation in all three parameters with a time-scale which, at first glance, seems consistent with the 321 d X-ray period of Bongiorno et al. (2011). This is better depicted in the right-hand panel of Fig. 4, where the Hα parameters are folded on the 321 d period. The plot also shows that the EWs of the MT and, in particular, the ST spectra are systematically lower than the rest. For comparison, Aragona et al. (2010) report EW = 52.3 Å on JD 245 4757–92. The FWHM and centroid velocities are again consistently lower in the MT and ST spectra. A plot of the average Hα profiles demonstrates that the line becomes weaker and narrower in the MT and ST spectra because of the gradual appearance of a broad absorption throat with a full-width zero-intensity FWZI ∼ 2000 km s^{-1} (see the bottom panel in Fig. 5). This is the characteristic of the faint states of Be stars which are likely related to episodes of the reduced circumstellar envelope (Grundstrom & Gies 2006). Broad absorptions are also detected in Hβ and the myriad of Fe II lines which plague the blue spectral range such as Fe II 4924 and 5018 Å (see the top panel in Fig. 5). These absorptions will likely contaminate most of the photospheric lines. Therefore, we decided to exclude these spectra from the study of the radial velocity curve of the Be star.

As in MWC 656, radial velocities were obtained by cross-correlating every blue INT/WHT/LT spectrum with a template produced from the average of all. Prior to this, each spectrum was rebinned into a uniform velocity scale of 23 km s^{-1} pixel^{-1}. Cross-correlation was performed over spectral windows covering the He I lines 4471, 4713 and 5048 Å. Additional regions containing lines of Si III (4568 and 4575 Å), C III/O II (4639–4650 Å) and He II 4686 Å were also included. These absorption features are stronger in MWC 148 than in MWC 656 because of its earlier spectral type. The rest velocity of the template was again determined through a Gaussian fit to the core of the He I 4471 Å line, and it was subsequently added to the cross-correlation velocities. The radial velocity curve, folded on the 321 d period, is displayed in Fig. 6. In spite of the limited phase coverage and velocity scatter, a sharp velocity minimum is detected. The narrowness of this feature prompts for a large eccentricity. We have attempted to model this radial velocity curve with the SBOP-fitting code, fixing the orbital period to 321 d. Following Bongiorno et al. (2011), we have defined phase 0 as HJD 2454857.5 which was arbitrarily set to the date of the first *Swift*/XRT observation in their paper. The best-fitting orbital elements are presented in the second column of Table 3.

6 DISCUSSION

In this paper we have presented an extensive spectroscopic data base of MWC 656 and MWC 148, the optical counterparts of the candidate γ-ray binaries AGL J2241+4454 and HESS J0632+057, respectively. Our data show evidence for long-term modulation in the main Hα parameters, consistent with the proposed orbital periods of 60.37 and 321 d, respectively. These modulations are likely produced by tidal instabilities in the circumstellar envelopes triggered by the motion of the compact star in an eccentric orbit. Circumstantial support for the orbital nature of the Hα variability is given by the EW values. The EW of the Hα line in Be/X-ray binaries provides a good estimate of the size of the circumstellar disc and, because this is truncated by the tidal torques of the compact star, a
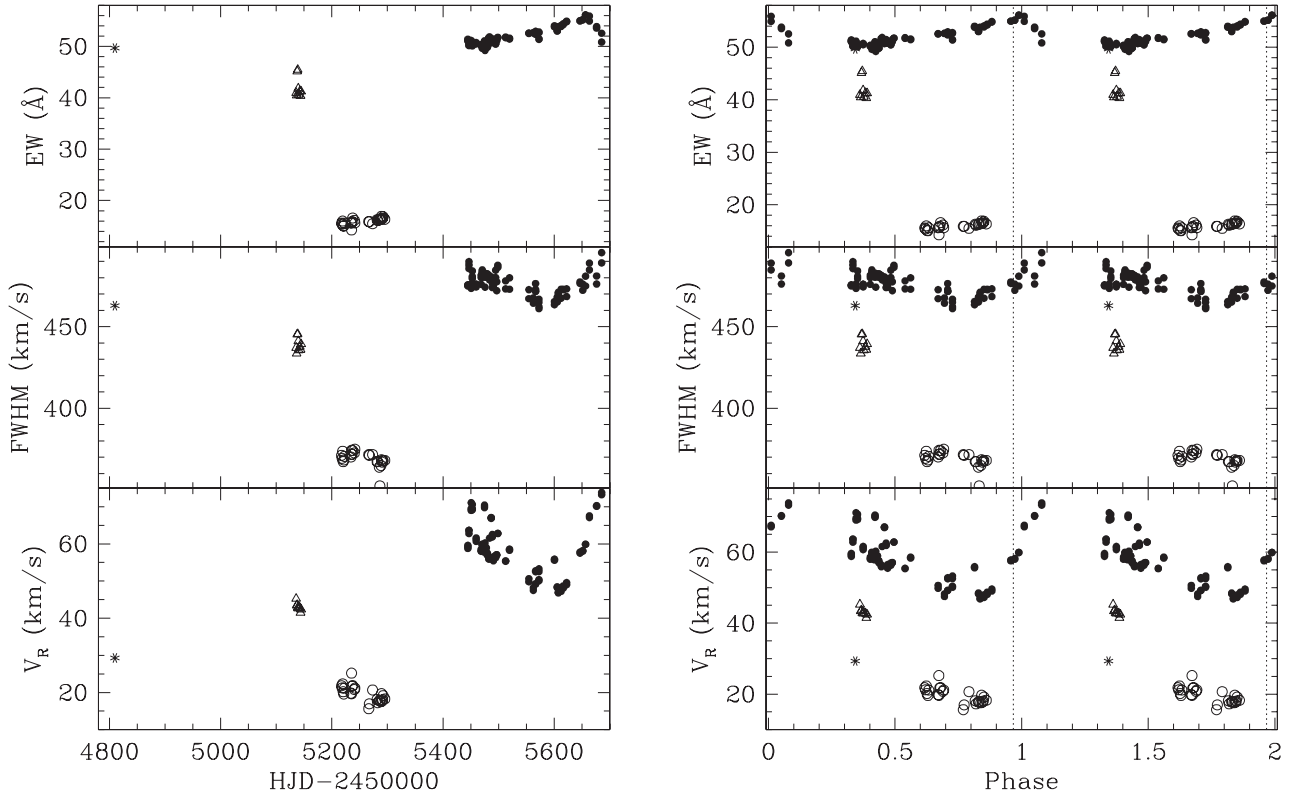
Figure 4. Left-hand panel: time evolution of the Hα line parameters in MWC 148. Different symbols indicate different data sets as follows: asterisk (WHT), open triangles (MT) open circles (ST) and filled circles (LT). Note the sinusoidal modulation in the LT data with a time-scale of ≈300 d. Error bars are not plotted because they are always smaller than the symbol size. Right-hand panel: same as in the left-hand panel but folded on the 321 d X-ray period of Bongiorno et al. (2011). Phase 0 has been set to HJD 2454857.5. Periastron is marked by a vertical dotted line (see the text).

simple relation EW(Hα) ∝ $P^{4/3}$ is expected (Reig 2011). It should be noted that this correlation holds for the maximum EW observed over a long length of time. We measure EW =25 Å for MWC 656 and 56 Å for MWC 148 which, according to the empirical P_{orb}−EW (Hα) diagram in fig.15 of Reig (2011), suggest P_{orb} ≈ 90 and 250 d, respectively. Given the scatter of the figure, these are fully consistent with the orbital periods proposed in the literature.

Figure 5. Average spectra of MWC 148 showing the evolution of several circumstellar disc profiles. The emission lines weaken because of the appearance of broad absorption throats, especially clear in the ST spectra.
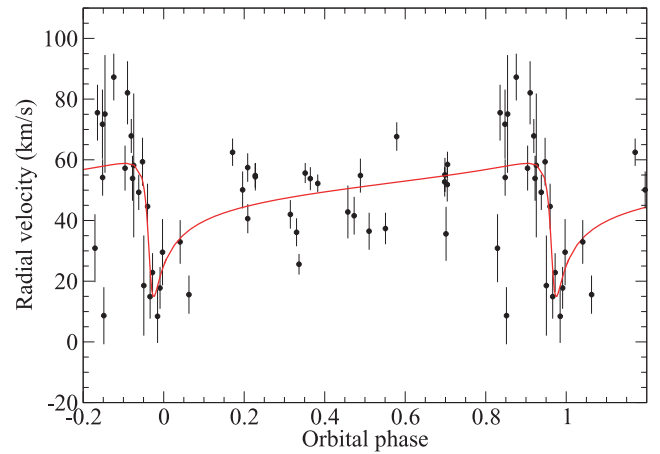

Figure 6. Radial velocity curve of MWC 148 folded on the 321 d period. The best eccentric orbital solution is overplotted. Phase 0 is set to HJD 2454857.5.

6.1 Masses of the compact stars

Furthermore, we have detected radial velocity variations in the photospheric lines of both MWC 656 and MWC 148. Assuming that their orbital periods are 60.37 d and 321 d, we produce phase-folded radial velocity curves which allows us to constrain their orbital elements for the first time. In particular, we determine the mass function of the compact object to be $f(M) = M_c^3 \sin^3 i/(M_c + M_{opt})^2 = 0.35^{+0.20}_{-0.15}$ M$_\odot$ for MWC 656 and $0.06^{+0.15}_{-0.05}$ M$_\odot$ for MWC 148. In this equation, M_c and M_{opt} stand for the masses of the compact and the optical star, respectively. Unfortunately, no pulsations have been detected from the compact stars yet and hence we cannot provide a full solution to the stellar masses and the nature of the invisible companions at this point. However, some speculations can be made based on our determination of the rotational broadenings $v \sin i$.

We measure $v \sin i \sim 346$ km s^{-1} for MWC 656 and ~ 373 km s^{-1} for MWC 148. A lower limit to the inclination can be derived from the condition that the optical companion should not exceed 0.9 times the critical rotational velocity v_{crit}. According to table 2 in Yudin (2001), $v_{crit} \sim 565$ km s^{-1} for a B0 V which implies $i \gtrsim 47°$ for MWC 148. On the other hand, $v_{crit} \sim 420$ km s^{-1} for a B3 IV and hence $i \gtrsim 66°$ for MWC 656. These estimates obviously assume that the Be star's spin axis and the orbital axis are aligned, which may not be true considering a possible kick during the supernova explosion that forms the compact object.

In addition, the presence of double-peaked emission profiles in our spectra also hints for a moderately high inclination. In particular, the Fe II lines are optically thin and their profiles reflect the Keplerian rotation in the emitting part of the Be disc (Hanuschik 1996). Therefore, we can use their FWZI to estimate the binary inclination through FWZI/2 $\times \sin i = (GM_{opt}/R_{opt})^{1/2}$. We measure FWZI ($\lambda 5018$) ~ 1300 km s^{-1} in MWC 148 and, using $M_{opt} \simeq 13.2$–19.0 M$_\odot$ and $R_{opt} \simeq 6.0$–9.6 R$_\odot$ from Aragona et al. (2010), we find $i \sim 71°$–$90°$. Regarding MWC 656 we measure FWZI ($\lambda 5018$) ~ 1000 km s^{-1} which, combined with $M_{opt} \simeq 5.8$–9.8 M$_\odot$ and $R_{opt} \simeq 4.7$–8.5 R$_\odot$ from Williams et al. (2010), yield $i \sim 70°$–$76°$. These estimates, however, should be regarded as mere upper limits because the region where the Fe II lines are produced is unlikely to extend down to the surface of the Be star.

We also note that the Fe II profiles do not exhibit deep central absorptions below the continuum characteristic of shell stars. Shell lines are thought to be produced by obscuration of the star by the circumstellar disc and are only observed at $i \geq 80°$ (Hanuschik 1996), which sets a rough upper limit to the inclination in both MWC 148 and MWC 656. In summary, crude values of $i \simeq 47°$–$80°$ for MWC 148 and $i \simeq 67°$–$80°$ for MWC 656 seem the most plausible given the available constraints at this point. Bringing the constraints to the inclination and the Be stellar masses from Williams et al. (2010) and Aragona et al. (2010) into the mass function equation results in $M_c \simeq 2.7$–5.5 M$_\odot$ for MWC 656 and 1.3–7.1 M$_\odot$ for MWC 148, although these numbers should be treated with caution because of the large uncertainties involved in this calculation. First, the binary inclinations are loosely constrained and need to be refined. Furthermore, our orbital solution is based on a limited data set which requires confirmation through a more extended baseline. In particular, observations of MWC 148 around the periastron at phase 0 are strongly encouraged. Unfortunately, the long orbital period coupled to the annual solar cycle means that the first opportunity for ground observations will not occur until 2015 March.

The wide range of masses allowed by our orbital solutions prevents us from deciding whether the compact objects in MWC 148 and MWC 656 are neutron stars or black holes. However, their long orbital periods place them among the widest γ-ray binaries, only after PSR B1259–63, and this offers an opportunity to probe the nature of the compact star through the detection of radio pulsations. Previous attempts in LS 5039 and LS I +61 303 have failed presumably due to strong free–free absorption by the dense stellar winds (see McSwain et al. 2011, and references therein). In principle, the detection of radio pulses might be possible in both MWC 148 and MWC 656 around apastron phases due to their wider orbits. X-ray pulses are also expected to arise through synchrotron emission in the magnetosphere of a rotationally powered pulsar or from an accreting neutron star. Deep searches for X-ray pulsations have been performed in both LS 5039 and LS I +61 303 with null results (see Rea et al. 2010, 2011, and references therein). This implies that the putative pulsars are spinning faster than ~ 5.6 ms, the pulsar beam is pointing away from our line of sight or X-ray pulsations are restricted to a limited range of orbital phases. We note that Rea et al. (2011) could not either find pulsations in MWC 148 using *Chandra* data during one outburst nor in *XMM–Newton* data during quiescence. These observations had a time resolution of only 199.2 ms and, according to our ephemeris, were performed at orbital phases 0.33 and 0.46, respectively. Therefore, the *XMM–Newton* data coincide with the apastron passage, where Compton scattering is lower and hence more favourable for the detection of X-ray pulses. More higher time-resolution observations of both MWC 656 and MWC 148 at different orbital phases are urgently required to test the nature of their compact stars.

6.2 Orbital variability

Aside from the stellar masses, our orbital solutions do provide interesting information on the geometry of the γ-ray binaries and properties of the observed X-ray/VHE radiation. Fig. 7 presents the relative motion of the compact star around the optical companion for both MWC 656 and MWC 148 as seen from above, i.e. $i = 0°$. The figure was produced using the stellar masses and radii from Williams et al. (2010) and Aragona et al. (2010) and assuming a 1.4 M$_\odot$ compact star. Our ephemeris imply that the X-ray outbursts in MWC 148 are delayed by ~ 100 d or 0.3 orbital phases with respect to the periastron passage. This is remarkably similar to LS I +61 303 where X-ray outbursts are observed ~ 0.2 orbital phases passed the closest approach of the stellar components (Casares et al. 2005a).

Regarding MWC 656, the maximum of the optical modulation takes place ~ 0.25 orbits after periastron. A similar phase shift of the photometric maximum is seen in LS I +61 303 (Mendelson & Mazeh 1989; Paredes et al. 1994). In addition, the right-hand frame in Fig. 2 shows that the EW of the Hα-line peaks ~ 0.3 orbital phases passed periastron. This behaviour seems consistent with a scenario where the modulation in both the continuum flux and the (optically thick) Hα flux is caused by the visibility of a one-arm tidal wave in the circumstellar disc, triggered by the close passage of the neutron star. For instance, Okazaki et al. (2002) present smoothed particle hydrodynamics simulations of a Be/X-ray binary with $P_{orb} = 24.3$ d and $e = 0.34$ which is not too far from the parameters that we derive for MWC 656. Their simulations (see figs 10 and 11 in the paper) show that a spiral density wave, excited by the periastron passage, is fully developed around phase ~ 0.25 past periastron. Furthermore, Williams et al. (2010) observed a rapid variability of the V/R ratio of the Hγ emission and suggested it could be associated with the changing tidal effects of the companion on the disc, which is specially strong near periastron. Indeed, these
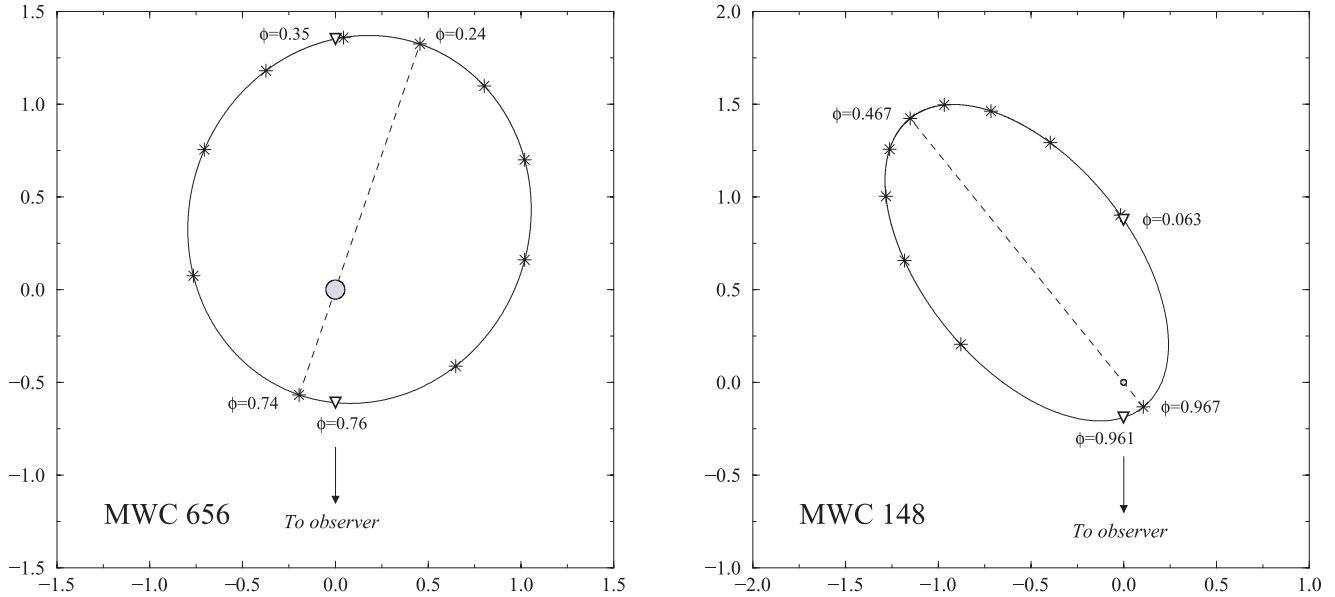
Figure 7. Left-hand panel: relative orbit of the compact object around the optical star in MWC 656 as seen from above the orbital plane. Phases of periastron and apastron are indicated and joined by a dashed line which depicts the major axis of the orbit. Stars mark 0.1 phase intervals from periastron whereas open triangles indicate the phases of the inferior conjunction and superior conjunction of the compact star. The coordinates are in units of the orbital semimajor axis. Right-hand panel: same for MWC 148. Note that the semimajor axis is 0.64 au in MWC 656 and 2.38 au in MWC 148.

observations correspond to orbital phases 0.82 ± 0.02 and 0.84 ± 0.02 which according to our ephemeris are just ~ 0.08 and ~ 0.10 in phase after periastron. At phase ~ 0.8, we also observe a rapid transition of the Hα centroid from negative to positive velocities, coincident with a peak in the FWHM (see the right-hand panel in Fig. 2).

In view of the new orbital ephemeris of MWC 656 it is also interesting to put in context the multiwavelength observations of the source. First of all, the *AGILE* detection between 2010 July 25 at 01:00 UT and 2010 July 26 at 23:30 UT (Lucarelli et al. 2010), corresponding to an orbital phase range of 0.77–0.80, took place just after (or even during) periastron. A maximum of the GeV emission takes place during periastron in LS 5039 (Abdo et al. 2009b) and soon after it in LS I +61 303 (Abdo et al. 2009a). The fact that the *AGILE* flare in MWC 656 occurs very close to the inferior conjunction of the compact object ($w = 71° \pm 23°$), coupled with its high orbital inclination, may explain the weak GeV emission through a reduction in the Compton scattering cross-section for large angles (Khangulyan, Aharonian & Bosch-Ramon 2008). All these facts reinforce the association between the Be star MWC 656 and the γ-ray source AGL J2241+4454 and, even with the lack of γ-ray detections aside from the flare seen by *AGILE* during a single periastron passage, give strong support to the idea that MWC 656 is a new γ-ray binary.

On the other hand, MWC 148 has only shown significant VHE radiation simultaneous to the X-ray flare episodes which occur ~ 0.3 phases past periastron. Indeed, according to our ephemeris, the Very Energetic Radiation Imaging Telescope Array System upper limits (Acciari et al. 2009) were obtained during the phase intervals 0.6–0.72, 0.86–0.93 and 0–0.01, corresponding to low levels of quiescent X-ray emission (Bongiorno et al. 2011). Conversely, the High Energy Stereoscopic System (HESS) discovery observations occurred at phases 0.32 and 0.36–0.46, coincident with periods of X-ray flares. Further detections of MWC 148 at VHE during X-ray active phases have been reported by Ong et al. (2011) and Mariotti et al. (2011).

6.3 The class of γ-ray binaries

The family of γ-ray binaries is growing fast with the recent discovery of AGL J2241+4454, HESS J0632+057.1 and 1FGL J1018.6−5856. These add up to the group of 'classic' γ-ray binaries PSR B1259−63, LS 5039 and LS I +61 303. Table 4 summarizes some of their main physical parameters. They all contain late-O–Be stars with strong winds and stellar radii in the range of $\sim$7–10 R$_\odot$. The table shows a possible correlation between the eccentricity and the orbital period and this is illustrated in Fig. 8. A least-squared linear fit yields

$$e = 0.206(19) \times \log P_{\mathrm{orb}} + 0.233(60). \qquad (1)$$

For comparison, Fig. 8 also presents 35 HMXBs with X-ray pulsars from Liu, van Paradijs & van den Heuvel (2006) and Martin, Tout & Pringle (2009). HMXBs tend to lie below the linear regression of γ-ray binaries, i.e. for a given orbital period they have lower eccentricities. The only exceptions are 4U 1850−03, 0535−668 and the Small Magellanic Cloud (SMC) binary J0045−7319, all with $e > 0.8$. In particular, the latter two have $P_{\mathrm{spin}} < 1$ s and hence a high spin-down power which makes them potential candidates for γ-ray emission.

The reason behind the P_{orb}–e correlation in γ-ray binaries stems from the fact that small stellar separations are required to trigger VHE radiation and this can only happen for long orbital periods if the eccentricity is large. Conversely, for short orbital periods high eccentricities would imply that the compact object passes through the stellar atmosphere of the companion, clearly an unstable situation. The separation of the two stars at periastron $a(1 - e)$ and apastron $a(1 + e)$ is also listed in Table 4, assuming that the compact star is a 1.4 M$_\odot$ neutron star. As expected, the most compact binaries LS 5039, 1FGL J1018.6−5856 and LS I +61 303 show persistent VHE and/or HE radiation modulated with their orbital periods, whereas only transient radiation is detected in PSR B1259−63 around periastron. This seems to imply that stellar separations $\lesssim 1$ au or $\lesssim 25$ R_{opt} are required for the efficient production and modulation of the

Table 4. The family of γ-ray binaries sorted by orbital period.

Name	γ-ray activity	Spectral type	M_{opt} ($M_\odot$)	R_{opt} ($R_\odot$)	i ($°$)	P_{orb} (d)	e	$a(1-e)$ (au)	$a(1+e)$ (au)	EW (Å)	d (kpc)	Reference[a]
LS 5039	HE, VHE	O6.5 V((f))	20–26	9–10	13–64	3.91	0.35	0.09	0.19	-2.8	2.5	(1)
1FGL J1018.6−5856	HE	O6 V((f))	~37	~10	–	16.58	–	–	–	–	~5.4	(2), (3)
LS I +61 303	HE, VHE	B0 Ve	10–15	~7	10–60	26.50	0.54	0.19	0.64	8–19	1.9	(4), (5), (6), (7)
MWC 656	HE	B3 IVne+sh	6–10	5–9	67–80	60.37	0.40	0.38	0.89	19–25	~2.6	(8), this paper
MWC 148	VHE	B0 Vpe	13–19	6–10	47–80	321	0.83	0.40	4.35	48–56	~1.4	(9), this paper
PSR B1259−63	HE, VHE	O9.5 Ve	31	9	19–31	1236.79	0.87	0.93	13.44	40–80	2.3	(10), (11), (12)

[a](1) Casares et al. (2005b). (2) Corbet et al. (2011). (3) Napoli et al. (2011). (4) Aragona et al. (2009). (5) Zamanov et al. (1999). (6) Casares et al. (2005a). (7) McSwain et al. (2010). (8) Williams et al. (2010). (9) Aragona et al. (2010). (10) Negueruela et al. (2011). (11) Johnston et al. (1994). (12) Grundstrom et al. (private communication).
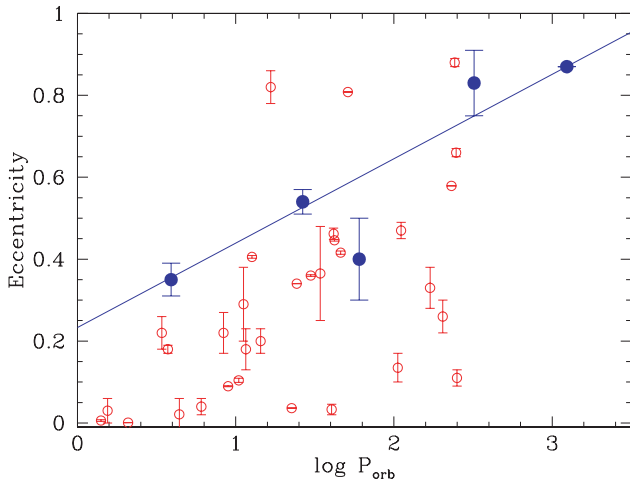
Figure 8. Eccentricity versus orbital period for γ-ray binaries (filled circles) and HMXBs from the catalogue of Liu et al. 2007 (open circles). A linear fit to the γ-ray binaries is overplotted.

Figure 9. Maximum EW of the Hα emission line versus orbital period for γ-ray binaries (filled circles) and Be/X-ray binaries (open circles). The latter include Milky Way and SMC binaries from Reig (2011). A linear fit to the γ-ray binaries is overplotted. Note that LS 5039 is not included because the primary is not a Be star.

HE/VHE radiation, but the picture is certainly more complex. For instance, MWC 656 has been detected up to GeV energies only once during a flare episode at periastron, whereas MWC 148 is regularly detected at TeV ~ 0.3 orbital phases past periastron. Aside from sensitivity limitations of different satellite/telescopes, other processes such as photon–photon annihilation and the subsequent production of electron–positron pairs are likely responsible for the wide phenomenology observed. In particular, the binary inclination and argument of periastron are important parameters for the attenuation of the VHE radiation and modelling the observed amplitudes (Dubus 2006).

It is well established that decretion discs in Be/X-ray binaries are truncated by the tidal torque of the neutron star (Negueruela & Okazaki 2001). Since the EW of the Hα emission is a good proxy of the disc size, this results in the well-known correlation between P_{orb} and the maximum observed EW (Hα) (Reig, Fabregat & Coe 1997; Reig 2011). Most γ-ray binaries contain Be primaries, and it is interesting to test whether a similar correlation holds. Table 4 lists the range of EW (Hα) values reported in the literature for the γ-ray binaries. Significant long-term and orbital variability is typically seen in Be/X-ray binaries and the same is observed in the γ-ray binaries. In this paper we detect a maximum EW for MWC 656 at ~ 0.3 phases past periastron, in agreement with what is observed in LS I +61 303 (McSwain et al. 2010). On the other hand, the maximum EW for MWC 148 occurs at periastron. In any case, only the maximum EW values are driven by the disc truncation radius.
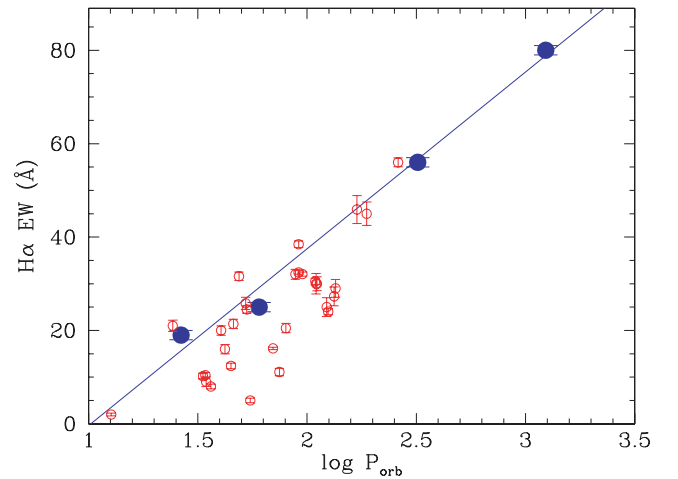
Fig. 9 plots the maximum EW (Hα) measured in γ-ray binaries with Be primaries versus P_{orb} and we note that they follow the linear regression:

$$EW = 37.8(5.0) \times \log P_{orb} - 38.3(11.4). \qquad (2)$$

For comparison, Fig. 9 also shows EWs of Be/X-ray binaries from Reig (2011). As in the case of the eccentricity, we observe that γ-ray binaries define the higher envelope of the distribution, i.e. for a given orbital period Be/X-ray binaries tend to have smaller decretion discs than γ-ray binaries. This is somehow surprising in a millisecond pulsar scenario because it implies that the relativistic pulsar wind does not 'erode' significantly the circumstellar disc even during the periastron passage. However, it is also true that, given the large eccentricities of γ-ray binaries, they only spend a short fraction of time close to the Be star, perhaps preventing efficient truncation. Interestingly, equations (1) and (2) provide a new tool for a rough estimate of two fundamental parameters (such as P_{orb} and e) in Be/γ-ray binaries simply from the EW of the Hα emission. This can be tested with future observations of newly discovered γ-ray binaries.

7 SUMMARY

We have reported optical spectroscopy of MWC 656 and MWC 148, the optical counterparts of the γ-ray sources AGL J2241+4454

and HESS J0632+057, respectively. Our data show that the main Hα parameters are modulated with the 60.37 d optical photometric period in MWC 656 and with the 321 d X-ray period in MWC 148. This is likely produced by the visibility of a tidal wave in the Be disc, triggered by the close passage of a compact star. In addition, we present radial velocity curves for the two stars and the first constraints to the binary parameters. Both stars display similarities with LS I +61 303, where photometric maxima and X-ray outburst are delayed by ∼0.3 phases past periastron. When compared to other γ-ray binaries, we find that the eccentricity is correlated with the orbital period. This is explained by the small stellar separations needed for triggering the γ-ray activity. The maximum EW of the Hα emission is also correlated with the orbital period. This is reminiscent of Be/X-ray binaries and suggest that the size of circumstellar discs in γ-ray binaries is tidally truncated by the compact companion.

8 ACKNOWLEDGMENTS

REFERENCES

Abdo A. A. et al., 2009a, ApJ, 701, L123
Abdo A. A. et al., 2009b, ApJ, 706, L56
Abt H. A., Levato H., Grosso M., 2002, ApJ, 573, 359
Acciari V. A. et al., 2009, ApJ, 698, L94
Aharonian F. A. et al., 2007, A&A, 469, L1
Aragona C., McSwain M. V., Grundstrom E. D., Marsh A. N., Roettenbacher R. M., Hessler K. M., Boyajian T. S., Ray P. S., 2009, ApJ, 698, 514
Aragona C., McSwain M. V., De Becker M., 2010, ApJ, 724, 306
Bongiorno S. D., Falcone A. D., Stroh M., Holder J., Skilton J. L., Hinton J. A., Gehrels N., Grube J., 2011, ApJ, 737, L11
Casares J., Ribas I., Paredes J. M., Martí J., Allende Prieto C., 2005a, MNRAS, 360, 1105
Casares J., Ribó M., Ribas I., Paredes J. M., Martí J., Herrero A., 2005b, MNRAS, 364, 899

Casares J. et al., 2011, in Rea N., Torres D. F., eds, Astrophysics and Space Science Proceedings, High-Energy Emission from Pulsars and their Systems. Springer-Verlag, Heidelberg, p. 559
Corbet R. H. D. et al., 2011, Astron. Telegram, 3221
Dhawan V., Mioduszewski A., Rupen M., 2006, in Belloni T., ed., Proc. VI Microquasar Workshop: Microquasars and Beyond. PoS, p. 52.1
Dubus G., 2006, A&A, 451, 9
Etzel P. B., 2004, SBOP: Spectroscopic Binary Orbit Program (San Diego State University)
Falcone A. D., Grube J., Hinton J., Holder J., Maier G., Mukherjee R., Skilton J., Stroh M., 2010, ApJ, 708, L52
Gray D. F., 1992, The Observation and Analysis of Stellar Photospheres. Cambridge Univ. Press, Cambridge
Grundstrom E. D., Gies D. R., 2006, ApJ, 651, L53
Gutiérrez-Soto J., Fabregat J, Suso J., Lanzara M., Garrido R., Hubert A.-M., Floquet M., 2007, A&A, 476, 927
Hanuschik R. W., Hummel W., Sutorius E., Dietle O., Thimm G., 1996, A&AS, 116, 309
Hinton J. A., Hofmann W., 2009, ARA&A, 47, 523
Hinton J. A. et al., 2009, ApJ, 690, L101
Horne K., 1986, PASP, 98, 609
Johnston S., Manchester R. N., Lyne A. G., Nicastro L., Spyromilio J., 1994, MNRAS, 268, 430
Khangulyan D., Aharonian F., Bosch-Ramon V., 2008, MNRAS, 383, 467
Liu Q. Z., van Paradijs J., van den Heuvel E. P. J., 2006, A&A, 455, 1165
Lucarelli F. et al., 2010, Astron. Telegram, 2761
Mariotti M. et al., 2011, Astron. Telegram, 3161
Marsh T. R., Robinson E. L., Wood J. H., 1994, MNRAS, 266, 137
Martin R. G., Tout C. A., Pringle J. E., 2009, MNRAS, 397, 1563
McSwain M. V., Grundstrom E. D., Gies D. R., Ray P. S., 2010, ApJ, 724, 379
McSwain M. V., Ray P. S., Ransom S. M., Roberts M. S. E., Dougherty S. M., Pooley G. G., 2011, ApJ, 738, 105
Mendelson H., Mazeh T., 1989, MNRAS, 239, 733
Moldón J., Ribó M., Paredes J. M., 2011a, A&A, 533, L7
Moldón J., Johnston S., Ribó M., Paredes J. M., Deller A. T., 2011b, ApJ, 732, L10
Napoli V. J., McSwain M. V., Boyer A. N. M., Roettenbacher R. M., 2011, PASP, 123, 1262
Negueruela I., Okazaki A. T., 2001, A&A, 369, 108
Negueruela I., Ribó M., Herrero A., Lorenzo J., Khangulyan D., Aharonian F. A., 2011, ApJ, 732, L11
Okazaki A. T., Bate M. R., Ogilvie G. I., Pringle J. E., 2002, MNRAS, 337, 967
Ong R. et al., 2011, Astron. Telegram, 3153
Paredes J. M. et al., 1994, A&A, 288, 519
Paredes J. M., 2011, Il Nuovo Cimento C, preprint (arXiv:1101.4843)
Porter J. M., Rivinius T., 2003, PASP, 115, 1153
Rea N., Torres D. F., 2011, ApJ, 737, L12
Rea N., Torres D. F., van der Klis M., Jonker P. G., Méndez M., Sierpowska-Bartosik A., 2010, MNRAS, 405, 2206
Rea N., Torres D. F., Caliandro G. A., Hadasch D., van der Klis M., Jonker P. G., Méndez M., Sierpowska-Bartosik A., 2011, MNRAS, 416, 1514
Reig P., Fabregat J., Coe M. J., 1997, A&A, 322, 193
Reig P., 2011, Ap&SS, 332, 1
Ribó M., Paredes J. M., Moldón J., Martí J., Massi M., 2008, A&A, 481, 17
Skilton J. L. et al., 2009, MNRAS, 399, 317
Townsend R. H. D., Owocki S. P., Ud-Doula A., 2007, MNRAS, 382, 139
Williams S. J., Gies D. R., Matson R. A., Touhami Y., Grundstrom E. D., Huang W., McSwain M. V., 2010, ApJ, 723, L93
Yudin R. V., 2001, A&A, 368, 912
Zamanov R. K., Martí J., Paredes J. M., Fabregat J., Ribó M., Tarasov A. E., 1999, A&A, 351, 543

This paper has been typeset from a TEX/LATEX file prepared by the author.